Nonlinear Dynamic Modeling of Spike Train Transformations for Hippocampal-Cortical Prostheses

Dong Song*, *Member, IEEE*, Rosa H. M. Chan, Vasilis Z. Marmarelis, *Fellow, IEEE*, Robert E. Hampson, Sam A. Deadwyler, and Theodore W. Berger, *Senior Member, IEEE*

Abstract—One of the fundamental principles of cortical brain regions, including the hippocampus, is that information is represented in the ensemble firing of populations of neurons, i.e., spatio-temporal patterns of electrophysiological activity. The hippocampus has long been known to be responsible for the formation of declarative, or fact-based, memories. Damage to the hippocampus disrupts the propagation of spatio-temporal patterns of activity through hippocampal internal circuitry, resulting in a severe anterograde amnesia. Developing a neural prosthesis for the damaged hippocampus requires restoring this multiple-input, multiple-output transformation of spatio-temporal patterns of activity. Because the mechanisms underlying synaptic transmission and generation of electrical activity in neurons are inherently nonlinear, any such prosthesis must be based on a nonlinear multiple-input, multiple-output model. In this paper, we have formulated the transformational process of multi-site propagation of spike activity between two subregions of the hippocampus (CA3 and CA1) as the identification of a multiple-input, multiple-output (MIMO) system, and proposed that it can be decomposed into a series of multiple-input, single-output (MISO) systems. Each MISO system is modeled as a physiologically plausible structure that consists of 1) linear/nonlinear feedforward Volterra kernels modeling synaptic transmission and dendritic integration, 2) a linear feedback Volterra kernel modeling spike-triggered after-potentials, 3) a threshold for spike generation, 4) a summation process for somatic integration, and 5) a noise term representing intrinsic neuronal noise and the contributions of unobserved inputs. Input and output spike trains were recorded from hippocampal CA3 and CA1 regions of rats performing a spatial delayed-nonmatch-to-sample memory task that requires normal hippocampal function. Kernels were expanded with Laguerre basis functions and estimated using a maximum-likelihood method. Complexity of the feedforward kernel was progressively increased to capture higher-order system nonlinear dynamics. Results showed higher prediction accuracies as kernel complexity increased. Self-kernels describe the nonlinearities within each input. Cross-kernels capture the nonlinear interaction between inputs. Second- and third-order nonlinear models were found to successfully predict the CA1 output spike distribution based on CA3 input spike trains. First-order, linear models were shown to be insufficient.

Index Terms—Feedback, hippocampus, Laguerre expansion, multiple-input, multiple-output system, spatio-temporal pattern, spike, time-rescaling theorem, Volterra kernel.

I. INTRODUCTION

THERE are essentially three classes of central nervous system neural prostheses currently under development and application. The first class attempts to compensate for loss of sensory input by replacing the transduction by primary sensory cells of physical energy from the environment into electrical stimulation of sensory nerve fibers (e.g., cochlear implant or artificial retina), or sensory cortex [1], [2]. The second class is designed to compensate for loss of motor control, and does so through functional electrical stimulation, in which preprogrammed stimulation protocols are used to activate muscular movement [3], [4], or to control robotic systems or computer cursors by "decoding" motor cortical command signals from the brain [5]–[10]. The third class of neural prostheses is designed to replace lost cognitive function, i.e., damage to central parts of the brain that are neither expressly sensory nor expressly motor, but are the basis of higher thought processes such as memory, language, planning, etc. This third class of prostheses presents unique challenges given that the solution requires replacing, not communication between sensory events and the brain, and not between the brain and robotics/computer systems, but instead, replacing communication between brain regions. A prosthesis for a central part of the brain must replace the damaged cells with biomimetic, silicon neurons having functional properties specific to those of the damaged neurons. In addition, such a prosthesis must both receive as inputs and send as outputs electrical activity from/to regions of the brain with which the damaged neurons previously communicated. Thus, a cognitive prosthesis is one that would replace the computational function of the damaged brain area, and restore the input-output transmission of that computational capacity to appropriate brain regions.

We are in the process of developing a cognitive prosthesis for the hippocampus [11], [12], a region of the brain responsible for the formation of new long-term memories [13]–[17]. We are considering conditions in which a part of the hippocampal intrinsic trisynaptic circuit is damaged or destroyed, which commonly occurs as a consequence of stroke (selective loss
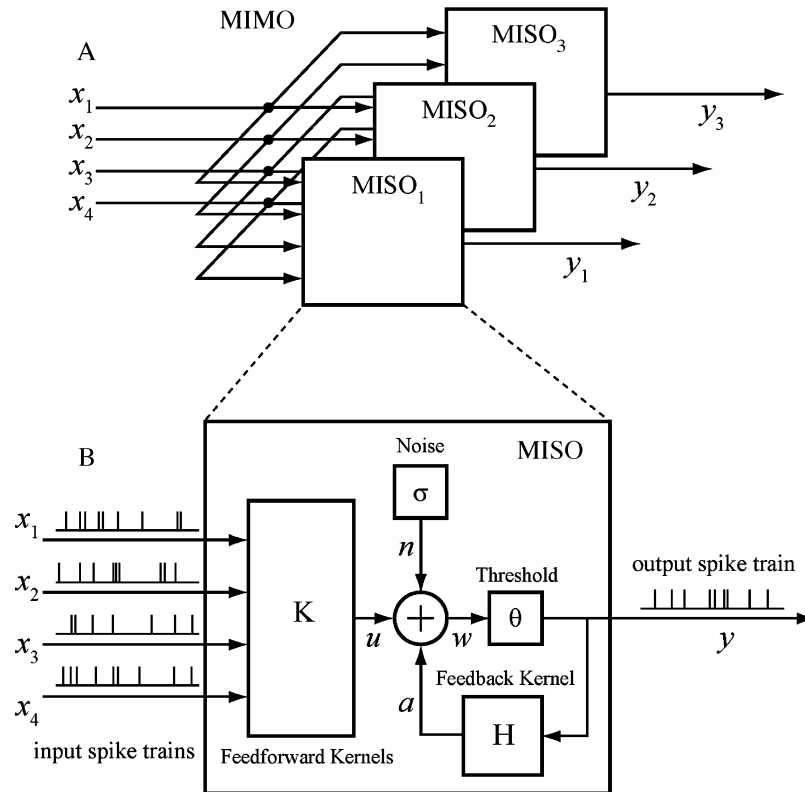
Fig. 1. General structure of MIMO and MISO models. (A) A MIMO model consists of a series of MISO models; (B) Each MISO model has a physiologically plausible structure. The K block contains feedforward kernels that can be of any order; The H block is the feedback kernel; n is a Gaussian white noise input with standard deviation σ; θ is a threshold; x denotes input spike trains; y denotes output spike trains; the hidden variable u is the "synaptic potential" w is the "prethreshold membrane potential"; a is the output spike-triggered "after-potential."

of CA1 neurons; [18]–[20]), epileptic activity (preferential damage to CA3; [21]), or head trauma (preferential damage to hippocampal hilar neurons; [22]). Alzheimer's Disease and other forms of dementia are consistently associated with loss of neurons throughout the hippocampal formation, though preferentially within the entorhinal layers providing inputs to, and receiving outputs from, the hippocampus proper [23]–[25]. As noted above, a critical part of achieving such a hippocampal prosthesis is a biomimetic replication of the computational/signal processing properties of the neurons to be replaced. The goal is to ensure that the prosthesis transforms input signals from one region of the hippocampus into appropriate output signals for another region of the hippocampus. For example, our previous steps in developing a hippocampal prosthesis have utilized the hippocampal slice. The transverse hippocampal slice preparation maintains intact the intrinsic trisynaptic pathway, including entorhinal cortical afferents to the dentate gyrus, dentate inputs to the CA3 region, and CA3 afferents to the CA1 layer. We developed a single-input, single-output model of the CA3 region, a hardware instantiation of that model, and a multi-electrode recording-stimulation array that supported bi-directional communication between the slice and the hardware model of CA3. The mathematical model of CA3 was experimentally based, and realized in the form of a truncated Volterra series (see [11] and below for more detail). In summary, the model predicts CA3 output on a msec-to-msec basis according to the past history (temporal pattern) of dentate input, and it does so for essentially all known physiological

dentate inputs and with approximately 95% accuracy. After surgical removal of CA3 from the slice, we demonstrated that the hardware-based input-output model successfully substituted for CA3 function, and reinstated trisynaptic circuit dynamics [11].

Our next step is to extend this approach to populations of neurons *in vivo*. One of the fundamental principles of cortical brain function in the behaving animal, including that of the hippocampus, is that information is represented in the ensemble firing of populations of neurons, i.e., spatio-temporal patterns of electrophysiological activity. For example, single neurons in primary visual cortex (V1) each respond maximally to linear visual stimuli of a given orientation; activity of the entire neuronal population provides a representation of the current visual field [26], [27]. Single neurons in primary motor cortex (M1) for the arm/hand region each respond maximally to given "reach" position in two- and three-dimensional space; activity of the entire neuronal population provides a representation of "reach space" [28], [29]. Representations in hippocampus can be more complex, with each neuron responding preferentially to a combination of multi-modal information related to extrinsic cues defining spatial location, learned behavior, and other factors [13], [14], [30]–[35]. Although there remains some debate as to the precise correlate of hippocampal neurons in behaving animals, it is the re-encoding of information as it propagates through hippocampal circuitry that allows the spatio-temporal patterns of activity representing short-term memory for events and/or labels ("declarative" information) to be converted into

the spatio-temporal patterns of activity appropriate for the formation of long-term memory [17], [35]–[37]. Thus, the essential challenge in developing a hippocampal neural prosthesis for the behaving animal is identifying a computational model that can accurately predict the nonlinear transformations of input hippocampal activity into output hippocampal activity to successfully re-instate the encoding of short-term memory into long-term memory.

This paper describes a modified Volterra kernel approach for such a modeling task. In this approach, the modeling of spatio-temporal pattern transformations is formulated as the identification of a multiple-input, multiple-output (MIMO) system that can be decomposed into a series of multiple-input, single-output (MISO) systems Fig. 1(A). Each MISO system is modeled by a physiologically plausible structure that is able to differentiate and capture feedforward and feedback nonlinear dynamics of the multiple intrinsic mechanisms and circuitries reflected in the activity of the output neuron in question Fig. 1(B). The feed-forward block of the model corresponds to the contribution of nonlinear synaptic transmission and dendritic integration of the neuron [38]–[40]. This block transforms input spike trains into a hidden variable, which can be interpreted as the postsynaptic potential. It is modeled by a nonlinear discrete-input, continuous-output Volterra kernel model. In addition to the feedforward component, a feedback block is included to model the spike-triggered processes that influence the future membrane potential and firing properties of the neuron. It is modeled by a linear first-order Volterra model. Previous electrophysiological and modeling studies have shown that spike-triggered processes can profoundly influence the firing behavior of hippocampal and other cortical neurons [41]–[46]. Furthermore, to assess the spiking variability caused by intrinsic neuronal noise and the contributions of unobserved inputs, a Gaussian white noise term is added to make the model stochastic.

Section II-A and B of this paper provide a brief description of the experimental procedures and data preprocessing. Sections II-C–II-F give detailed mathematical expressions of model configuration, parameter estimation, kernel reconstruction, and model validation. Models estimated from experimental data appear in Section III. Finally, we will discuss the possible extension of the model in Section IV.

II. METHODS

A. Experimental Procedures

Male Long-Evans rats were trained to criterion on a two-lever, spatial delayed-nonmatch-to-sample (DNMS) task with randomly occurring variable delay intervals [37], [47]. Animals performed the task by pressing (sample response) a single lever presented in one of the two positions in the sample phase (left or right); this event is called the "sample response." The lever was then retracted and the delay phase initiated; for the duration of the delay phase, the animal was required to nosepoke into a lighted device on the opposite wall. Following termination of the delay the nosepoke light was extinguished, both levers were extended and the animal was required to press the lever opposite to the sample lever; this act is called the "nonmatch response." If the correct lever was pressed, the animal was rewarded and the trial was completed.
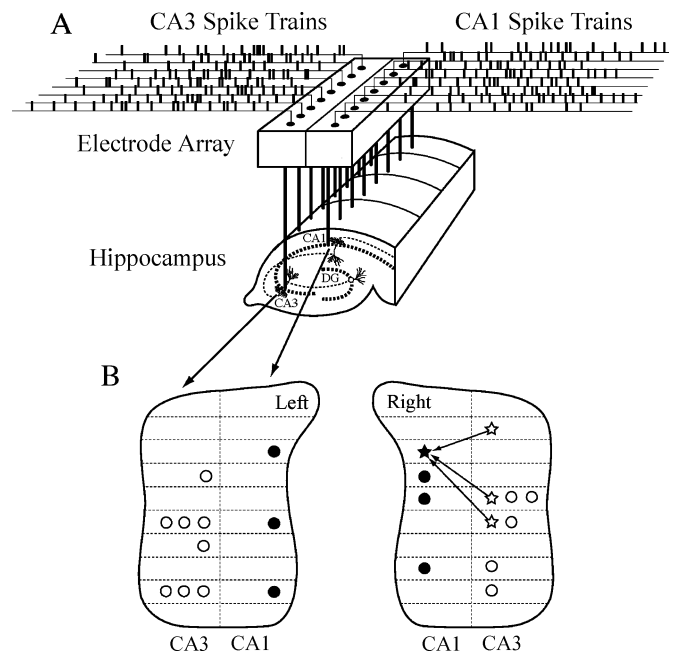

Fig. 2. Input and output signals of the model correspond to the spike trains recorded from hippocampal CA3 and CA1 regions. (A) CA3 and CA1 spike trains are recorded using a multi-electrode array. (B) Anatomical locations of input (CA3) and output (CA1) neurons indicated on a "foldout map" of the hippocampus (compare the CA3 and CA1 regions in (A) versus (B); after Swanson *et al.* [57]. For this sample MIMO dataset, there are 16 inputs (white symbols) and 7 outputs (black symbols). The sample MISO dataset illustrated has 3 inputs (white stars) and 1 output (black star).

Spike trains were obtained with multi-site recordings from different septo-temporal regions of the hippocampus of rats performing the above described DNMS task Fig. 2(A). For each hemisphere of the brain, an array of electrodes (microwires) was surgically implanted into the hippocampus, with 8 electrodes in the CA3 (input) region and 8 electrodes in the CA1 (output) region. Each electrode had the capacity of recording as many as 4 discriminable units. Spike and behavioral responses were digitized and time-stamped with a 25 μs resolution. Datasets from 6 rats were analyzed. Three sessions of recordings were selected from each rat. A session included approximately 90 successfully performed DNMS tasks that each consisted of four behavioral events, i.e., right sample (RS), left sample (LS), right nonmatch (RN), and left nonmatch (LN).

B. Data Preprocessing

Spike trains were prescreened based on mean firing rate and peri-event histogram. Neurons with mean firing rates in the range of 0.5 to 15 Hz and identifiable perievent histograms were included in further analyses. Low (<0.5 Hz) and high (>15 Hz) mean rate recordings were rejected since they could represent artifacts or mixtures of action potentials. Both presumed principal (pyramidal) neurons and interneurons were included in the datasets analyzed. The bin size was increased to 2 ms to reduce data length; for this bin size, each bin contained a maximum of one spike event. Perievent (−2 s to +2 s) spike trains of the four behavioral events were extracted from each session and then concatenated.

Each MIMO dataset consisted of between 6–16 CA3 spike trains and 5–10 CA1 spike trains, depending on the number of

neurons recorded from each animal and the number of recorded neurons meeting the selection criteria. Each MIMO dataset was divided into MISO datasets for system identification. Thus, for each CA1 output neuron from the set of output neurons recorded from a given animal, the MISO dataset included all CA3 spike trains recorded simultaneously. Fig. 2(B) shows the anatomical locations of neurons included in one representative MIMO dataset (all stars and circles) and one MISO dataset (stars) for illustration. Forty-two MISO datasets from 6 rats were analyzed.

C. Model Configuration

The MISO model has a physiologically plausible structure [Fig. 1(B)] that can be expressed by the following equations:

$$w = u(k, x) + a(h, y) + n(\sigma)$$

$$y = \begin{cases} 0, & \text{when } w < \theta \\ 1, & \text{when } w \geq \theta \end{cases}.$$

The variable x represents input spike trains; y represents output spike train. The hidden variable w represents the prethreshold potential of the output neurons. It is equal to the summation of three components, i.e., synaptic potential u caused by input spike trains, the output spike-triggered after-potential a, and a Gaussian white noise n with standard deviation σ. The noise term models both intrinsic noise of the output neuron and the contribution from unobserved inputs. When w crosses threshold θ, an output spike is generated and a feedback after-potential (a) is triggered and then added to w. Feedforward kernels k describe the transformation from x to u. The feedback kernel h describes the transformation from y to a.

u can be expressed as a Volterra functional series of x [48]–[51], as in

$$u(t) = k_0 + \sum_{n=1}^{N} \sum_{\tau=0}^{M_k} k_1^{(n)}(\tau) x_n(t - \tau)$$

$$+ \sum_{n=1}^{N} \sum_{\tau_1=0}^{M_k} \sum_{\tau_2=0}^{M_k} k_{2s}^{(n)}(\tau_1, \tau_2) x_n(t - \tau_1) x_n(t - \tau_2)$$

$$+ \sum_{n_1=1}^{N} \sum_{n_2=1}^{n_1-1} \sum_{\tau_1=0}^{M_k} \sum_{\tau_2=0}^{M_k} k_{2x}^{(n_1, n_2)}(\tau_1, \tau_2)$$

$$\times x_{n_1}(t - \tau_1) x_{n_2}(t - \tau_2)$$

$$+ \sum_{n=1}^{N} \sum_{\tau_1=0}^{M_k} \sum_{\tau_2=0}^{M_k} \sum_{\tau_3=0}^{M_k} k_{3s}^{(n)}(\tau_1, \tau_2, \tau_3)$$

$$\times x_n(t - \tau_1) x_n(t - \tau_2) x_n(t - \tau_3) + \dots$$

The zeroth-order kernel, k_0, is the value of u when the input is absent. First-order kernels, $k_1^{(n)}$, describe the linear relation between the nth input x_n and u. Second- and third-order self-kernels, $k_{2s}^{(n)}$ and $k_{3s}^{(n)}$, describe the second- and third-order non-linear relation between the nth input x_n and u, respectively. Second-order cross-kernels $k_{2x}^{(n_1, n_2)}$ describe the second-order nonlinear interactions between each unique pair of inputs x_{n_1} and x_{n_2} as they affect u. N is the number of inputs. M_k denotes the memory length of the feedforward process. Higher order kernels, e.g., third-order cross-kernels and fourth-order kernels, were not calculated in this study.

The feedback variable a can be expressed as

$$a(t) = \sum_{\tau=1}^{M_h} h(\tau) y(t - \tau)$$

where h is the linear feedback kernel. M_h is the memory of the feedback process.

In order to reduce the number of open parameters to be estimated, both k and h are expanded with orthonormal Laguerre basis functions b [52]

$$b_j(\tau) = \begin{cases} (-1)^{\tau} \alpha^{(j-\tau)/2} (1-\alpha)^{1/2} \\ \quad \times \sum_{k=0}^{\tau} (-1)^k \binom{\tau}{k} \binom{j}{k} \alpha^{\tau-k}(1-\alpha)^k & (0 \leq \tau < j) \\ (-1)^j \alpha^{(\tau-j)/2}(1-\alpha)^{1/2} \\ \quad \times \sum_{k=0}^{j} (-1)^k \binom{\tau}{k} \binom{j}{k} \alpha^{j-k}(1-\alpha)^k & (j \leq \tau \leq M) \end{cases}.$$

With input and output spike trains x and y convolved with b

$$v_j^{(n)}(t) = \sum_{\tau=0}^{M_k} b_j(\tau) x_n(t - \tau), \quad v_j^{(h)}(t) = \sum_{\tau=1}^{M_h} b_j(\tau) y(t - \tau).$$

u and a can be rewritten into:

$$u(t) = c_0 + \sum_{n=1}^{N} \sum_{j=1}^{L} c_1^{(n)}(j) v_j^{(n)}(t)$$

$$+ \sum_{n=1}^{N} \sum_{j_1=1}^{L} \sum_{j_2=1}^{j_1} c_{2s}^{(n)}(j_1, j_2) v_{j_1}^{(n)}(t) v_{j_2}^{(n)}(t)$$

$$+ \sum_{n_1=1}^{N} \sum_{n_2=1}^{n_1-1} \sum_{j_1=0}^{L} \sum_{j_2=0}^{L} c_{2x}^{(n_1, n_2)}(j_1, j_2) v_{j_1}^{(n)}(t) v_{j_2}^{(n)}(t)$$

$$+ \sum_{n=1}^{N} \sum_{j_1=1}^{L} \sum_{j_2=1}^{j_1} \sum_{j_3=1}^{j_2} c_{3s}^{(n)}(j_1, j_2, j_3) v_{j_1}^{n}(t) v_{j_2}^{n}(t) v_{j_3}^{n}(t)$$

$$+ \dots$$

$$a(t) = \sum_{j=1}^{L} c_h(j) v_j^{(h)}(t).$$

$c_1^{(n)}, c_{2s}^{(n)}, c_{2x}^{(n_1, n_2)}, c_{3s}^{(n)}$, and c_h are the sought Laguerre expansion coefficients of $k_1^{(n)}, k_{2s}^{(n)}, k_{2x}^{(n_1, n_2)}, k_{3s}^{(n)}$, and h, respectively (C_0 is simply equal to k_0). Since the number of basis functions (L) can be made much smaller than the memory length (M_k and M_h), the number of open parameters is greatly reduced by the expansion.

D. Parameter Estimation

With recorded input and output spike trains x and y, model parameters can be estimated using maximum-likelihood method. The log likelihood function L can be expressed as

$$L(y|x, k, h, \sigma, \theta) = \ln \prod_{t=0}^{T} P(y|x, k, h, \sigma, \theta)$$

$$= \sum_{t=0}^{T} \ln P(y|x, k, h, \sigma, \theta)$$

where

$$P(y|x,k,h,\sigma,\theta)=\begin{cases} \text{Prob}(w \ge \theta|x,k,h,\sigma,\theta), & \text{when } y=1 \\ \text{Prob}(w < \theta|x,k,h,\sigma,\theta), & \text{when } y=0 \end{cases}.$$

P can be calculated using error function (integral of Gaussian function)

$$P(t) = 0.5 - 0.5A(t)\text{erf}\left(\frac{\theta - w(t)}{\sqrt{2}\sigma}\right)$$

where $\text{erf}(s)$ and $A(t)$ are defined as

$$\text{erf}(s) = \frac{2}{\sqrt{\pi}}\int_0^s e^{-t^2}\,dt$$

$$A(t) = \begin{cases} +1, & \text{when } y=1 \\ -1, & \text{when } y=0 \end{cases}.$$

The gradient of log-likelihood function against coefficents c is given as

$$G(i) = \frac{\partial L}{\partial c_i} = \sum_{t=0}^{T} \frac{1}{P(t)} \cdot \frac{\partial P(t)}{\partial c_i}$$

$$= \sum_{t=0}^{T} \frac{1}{\sigma\sqrt{2\pi}P(t)}A(t)e^{-\frac{(\theta-w(t))^2}{2\sigma^2}} \cdot \frac{\partial w(t)}{\partial c_i}$$

where

$$\frac{\partial w(t)}{\partial c_0} = 1, \quad \frac{\partial w(t)}{\partial c_1^{(n)}(j)} = v_j^{(n)}(t)$$

$$\frac{\partial w(t)}{\partial c_{2s}^{(n)}(j_1,j_2)} = v_{j_1}^{(n)}(t)v_{j_2}^{(n)}(t)$$

$$\frac{\partial w(t)}{\partial c_{2x}^{(n_1,n_2)}(j_1,j_2)} = v_{j_1}^{(n_1)}(t)v_{j_2}^{(n_2)}(t)$$

$$\frac{\partial w(t)}{\partial c_{3s}^{(n)}(j_1,j_2,j_3)} = v_{j_1}^{(n)}(t)v_{j_2}^{(n)}(t)v_{j_3}^{(n)}(t)$$

$$\frac{\partial w(t)}{\partial c_h(j)} = v_j^{(h)}(t).$$

Hessian matrix H is given as

$$H(i,j) = \frac{\partial^2 L}{\partial c_i \partial c_j}$$

$$= \sum_{t=0}^{T}\left(-\frac{1}{P(t)^2}\cdot\frac{\partial P(t)}{\partial c_i}\cdot\frac{\partial P(t)}{\partial c_j} + \frac{1}{P(t)}\cdot\frac{\partial^2 P(t)}{\partial c_i \partial c_j}\right)$$

$$= \sum_{t=0}^{T} \frac{1}{\sigma\sqrt{2\pi}P(t)}A(t)e^{\frac{-(\theta-w(t))^2}{2\sigma^2}}$$

$$\times \left(\frac{-1}{\sigma\sqrt{2\pi}P(t)}A(t)e^{\frac{-(\theta-w(t))^2}{2\sigma^2}} + \frac{\theta-w(t)}{\sigma^2}\right)$$

$$\cdot \frac{\partial w(t)}{\partial c_i}\cdot\frac{\partial w(t)}{\partial c_j}.$$

Variables $c_1^{(n)}$, $c_{2s}^{(n)}$, $c_{2x}^{(n_1,n_2)}$, $c_{3s}^{(n)}$, c_h and $\theta - c_0$, which is the distance between the threshold and the baseline value of w, can be arbitrarily scaled without influencing the relation between x and y. Furthermore, θ and c_0 also can be shifted together. So

without loss of generality, both θ and σ can be set to unity value; only c are estimated. σ is later restored and θ remains unity value (see Section II-E). In this paper, both standard Newton nonlinear optimization method and generalized linear model (GLM) fitting method were used to estimate c by maximizing the likelihood function L [53]–[55]. Nearly identical results were obtained using these two methods, with the link function of GLM chosen to be the *probit* function, i.e., inverse cumulative distribution function of the normal distribution [55]. Confidence bounds of kernel coefficients are also estimated from the Hessian matrix. All the kernels shown in this paper have narrow 95% confidence bounds, which are not shown in the figures.

E. Kernel Reconstruction

The final coefficients $\hat{c}$ and $\hat{\sigma}$ can be obtained from estimated Laguerre expansion coefficients, $\tilde{c}$, with a simple normalization procedure

$$\hat{c}_0 = 0, \; \hat{c}_1^{(n)} = \frac{\tilde{c}_1^{(n)}}{1-\tilde{c}_0}, \; \hat{c}_{2s}^{(n)} = \frac{\tilde{c}_{2s}^{(n)}}{1-\tilde{c}_0}$$

$$\hat{c}_{2x}^{(n_1,n_2)} = \frac{\tilde{c}_{2x}^{(n_1,n_2)}}{1-\tilde{c}_0}, \; \hat{c}_{3s}^{(n)} = \frac{\tilde{c}_{3s}^{(n)}}{1-\tilde{c}_0}$$

$$\hat{c}_h = \frac{\tilde{c}_h}{1-\tilde{c}_0}, \; \hat{\sigma} = \frac{1}{1-\tilde{c}_0}$$

Feedforward and feedback kernels then can be reconstructed as

$$\hat{k}_0 = 0$$

$$\hat{k}_1^{(n)}(\tau) = \sum_{j=1}^{L}\hat{c}_1^{(n)}(j)b_j(\tau)$$

$$\hat{k}_{2s}^{(n)}(\tau_1,\tau_2) = \sum_{j_1=1}^{L}\sum_{j_2=1}^{j_1}\frac{\hat{c}_{2s}^{(n)}(j_1,j_2)}{2}$$

$$\times (b_{j1}(\tau_1)b_{j2}(\tau_2) + b_{j2}(\tau_1)b_{j1}(\tau_2))$$

$$\hat{k}_{2x}^{(n_1,n_2)}(\tau_1,\tau_2) = \sum_{j_1=1}^{L}\sum_{j_2=1}^{L}\hat{c}_{2x}^{(n_1,n_2)}(j_1,j_2)b_{j1}(\tau_1)b_{j2}(\tau_2)$$

$$\hat{k}_{3s}^{(n)}(\tau_1,\tau_2,\tau_3) = \sum_{j_1=1}^{L}\sum_{j_2=1}^{j_1}\sum_{j_3=1}^{j_2}\frac{\hat{c}_{3s}^{(n)}(j_1,j_2,j_3)}{6}$$

$$\times (b_{j1}(\tau_1)b_{j2}(\tau_2)b_{j3}(\tau_3)$$

$$+ b_{j1}(\tau_1)b_{j3}(\tau_2)b_{j2}(\tau_3)$$

$$+ b_{j2}(\tau_1)b_{j1}(\tau_2)b_{j3}(\tau_3)$$

$$+ b_{j2}(\tau_1)b_{j3}(\tau_2)b_{j1}(\tau_3)$$

$$+ b_{j3}(\tau_1)b_{j1}(\tau_2)b_{j2}(\tau_3)$$

$$+ b_{j3}(\tau_1)b_{j2}(\tau_2)b_{j1}(\tau_3))$$

$$\hat{h}(\tau) = \sum_{j=1}^{L}\hat{c}_h(j)b_j(\tau).$$

Threshold θ is equal to one in this normalized representation.

F. Model Validation and Prediction

The kernel models described in this paper generate output spike trains stochastically due to the inclusion of a noise term in the model. Thus, given the same input spike trains, output spike trains predicted by the kernel models are different each time.

This behavior makes direct comparison, e.g., mean-square error, between recorded output y and predicted output $\hat{y}$ difficult. Two indirect methods were used to evaluate the goodness-of-fit of the estimated models in this paper. To avoid overfitting, different datasets were used for parameter estimation and model validation in this study.

The first method evaluates the firing probability predicted by the model with the recorded output spike train. According to the time-rescaling theorem well-known in probability theory, an accurate model should generate a conditional firing intensity function that can transform the recorded output spike train into a Poisson process with unit rate [56]. The conditional firing intensity function P_f can be given as

$$P_f(t) = 0.5 - 0.5\mathrm{erf}\left(\frac{\theta - w(t)}{\sqrt{2}\sigma}\right).$$

This P_f is different from the P previously shown in the likelihood function, because the former represents the probability of generating a spike at a certain time t, whereas the latter denotes the probability of generating the recorded output y at time t. Let t_i denote the time of the ith spike in y, then according to the time-rescaling theorem

$$D(t_i) = \sum_{t=0}^{t_i} P_f(t),$$

should be a Poisson process with unit rate and its intervals,

$$\tau_f(i) = D(t_i) - D(t_{i-1}) = \sum_{t=t_{i-1}+1}^{t_i} P_f(t),$$

are independent exponential random variables with unitary mean. By making the further transformation

$$z(i) = 1 - e^{-\tau_f(i)}$$

then z are independent uniform random variables on the interval $(0, 1)$. The model goodness-of-fit then can be assessed with a Kolmogorov-Smirnov (KS) test, in which z are ordered from the smallest to the largest and then plotted against the cumulative distribution function of the uniform density defined as

$$\tilde{z}(i) = \frac{i - 0.5}{n}$$

where $i = 1, \ldots, n$ and n is the total number of output spikes. If the model is correct, all points should lie on the $45°$ line of the KS plot within the 95% confidence bounds given as $\tilde{z}(i) \pm 1.36/\sqrt{n}$ [56].

The second method quantifies the similarity between the recorded output spike train y and the predicted output spike train $\hat{y}$ after a smoothing process. First, $\hat{y}$ is predicted through simulation: u is calculated with input spike trains x and the estimated feedforward kernels $\hat{k}$. This forms the deterministic part of w. Then, a Gaussian random sequence with standard deviation $\hat{\sigma}$ is generated and added to u to obtain w. This

operation includes the stochastic component into w. At time t, if the value of w is higher than the threshold ($\theta = 1$)), a spike is added to $\hat{y}$ and a feedback component a is added to the future values of w. The calculation then repeats for time $t + 1$ with updated w until it reaches the end of the trace. Discrete signals $\hat{y}$ and y then are smoothed to continuous signals $\hat{y}_{\sigma_g}$ and y_{σ_g}, by convolution with a Gaussian kernel function having the standard deviation σ_g. Correlation (similarity) coefficients r then is calculated as

$$r(\sigma_g) = \frac{\sum_{t=0}^{T} \hat{y}_{\sigma_g}(t)y_{\sigma_g}(t)}{\sqrt{\left(\sum_{t=0}^{T} y_{\sigma_g}(t)y_{\sigma_g}(t)\right)\left(\sum_{t=0}^{T} \hat{y}_{\sigma_g}(t)\hat{y}_{\sigma_g}(t)\right)}}.$$

Because $\hat{y}_{\sigma_g}$ and y_{σ_g} are both positive vectors, r is a number between 0 and 1 that measures the similarity between $\hat{y}$ and y as a function of the "smoothness parameter" σ_g. r can be interpreted as the cosine of the angle between vectors $\hat{y}_{\sigma_g}$ and y_{σ_g}. In this paper, σ_g varies from 2 ms to 40 ms with a 2 ms resolution. For a given σ_g, r was estimated with 32 trials of simulation of $\hat{y}$.

III. RESULTS

MIMO models are estimated as arrays of their corresponding MISO models consistent with the spatio-temporal pattern structure of the hippocampus, i.e., transformations of inputs from multiple CA3 neurons to a given CA1 neuron. Thus, estimating each MIMO model requires estimating the first-order kernels, second-order self-kernels, second-order cross-kernels, and third-order self-kernels for each of the MISO models comprising the MIMO set (Fig. 1). Each kernel model contains all the lower order terms, e.g., third-order self-kernel model has first-order, second-order self and cross-terms and, thus, is a superset of the lower order kernel models. The feedback kernel h is limited to the linear case (first-order) in all models.

A. First-Order Kernel MISO Model

The feedforward process [K in Fig. 1(B)] is linear in the first-order kernel model. Fig. 3 shows k_1 of a representative first-order MISO model with 3 inputs. The locations of the input and output neurons are shown in Fig. 2(B) (stars). k_1 are vectors with length M_k. The Gaussian noise standard deviation σ is estimated to be 0.311. The KS plot shows that the first-order MISO model displays a lack of fit for the lower half of quantiles (0.2–0.6), because in that range, model values lie outside the 95% confidence bounds Fig. 4(C). The maximum distance between model values and the $45°$ line is 0.157. A similar insufficiency of first-order models was found in all MISO datasets (42 of 42).

B. Second-Order Self-Kernel MISO Model

The second-order self-kernel model has second-order terms for each individual input. k_{2s} are $M_k \times M_k$ symmetric matrices describing the pair-wise nonlinear interaction between spikes of the same input as they affect the hidden variable u (Fig. 5, bottom row). The noise term, σ was estimated to be 0.298. Including the second-order self-nonlinearities in the model significantly increased the accuracy of the model, as shown by the increased log likelihood value Fig. 4(A). In the KS plot for the
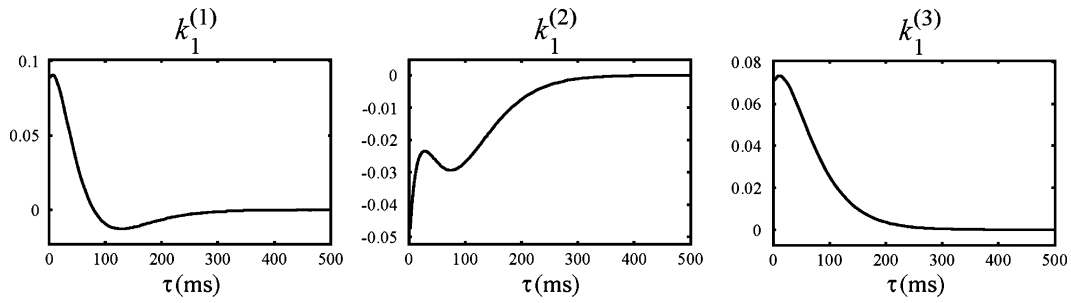
Fig. 3. Feedforward kernels (block K in Fig. 1) of the first-order kernel model of a 3-input MISO dataset. These first-order kernels (k_1) describe the linear transformation of input spikes trains (x) into the hidden variable u, as functions of the time intervals between present time and the previous spikes (τ). Each figure corresponds to one input.
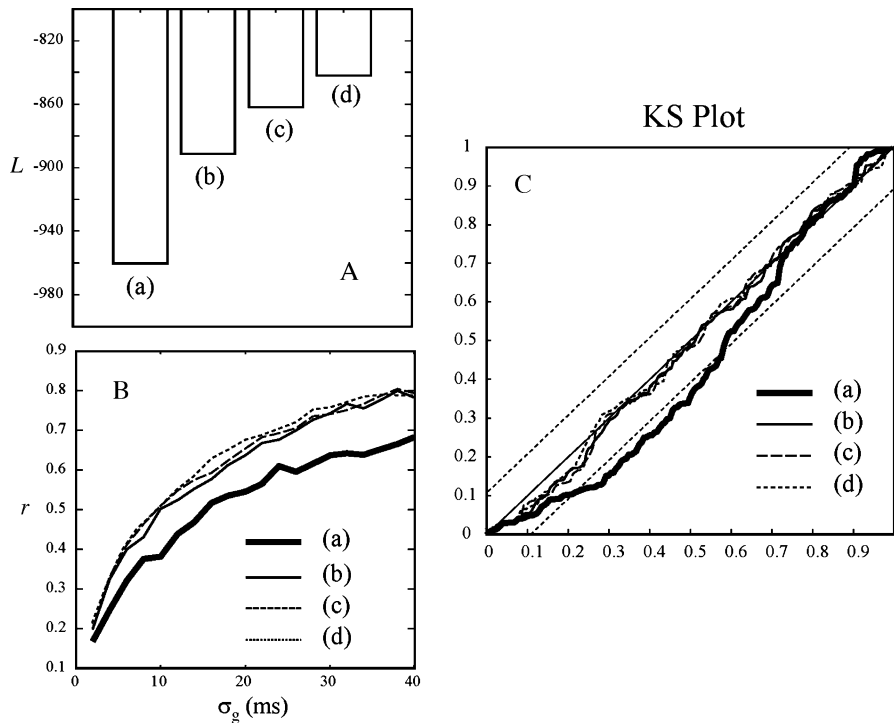

Fig. 4. (A) Log Likelihood L, (B) Correlation coefficients r, and (C) KS plots, of (a) first-order kernel model, (b) second-order self-kernel model, (c) second-order cross-kernel model, and (d) third-order self-kernel model. Straight dashed lines in KS plot are the 95% confidence bounds.

second-order self-kernel models, all values lay within the 95% confidence bound Fig. 4(C). The maximum distance between model values and the 45° line is 0.063. Similar KS results were obtained in 85% of the MISO datasets (36 of 42).

C. Second-Order Cross-Kernel MISO Model

The second-order cross-kernel model has additional cross-terms for each pair of inputs. There are 3 cross-kernels in the 3-input model (Fig. 6, bottom row). k_{2x} are $M_k \times M_k$ asymmetric matrices describing the interactions between pairs of spike inputs occurring on different inputs as they affect u. The noise term, σ was estimated to be 0.295. This inclusion of additional nonlinearities further increased the log likelihood Fig. 4(A). The KS plot for model results including second-order cross nonlinearities shows that all values lay within the 95% confidence bound Fig. 4(C). The maximum distance between

model values and the 45° line is 0.061. All MISO datasets showed similar results (42 of 42).

D. Third-Order Self-Kernel MISO Model

The third-order self-kernel model includes additional third-order terms for each input (Fig. 7, bottom 3 rows). k_{3x} are $M_k \times M_k \times M_k$ symmetric matrices describing the interaction between triplet of spikes from the same input as they affect u. Because the third-order kernel has a four dimensional data structure, only "slices" of the third-order kernel, or third-order kernel for a selected "third" inter-spike interval, are shown here. In Fig. 7, k_{3x} are shown for 3 selected time lags (20, 40 and 60 ms; rows 4–6). The noise term, σ was estimated to be 0.295. The third-order self-kernel model has the highest log likelihood value of the four models [Fig. 4(A)]. The KS plot for the third-order model results displays values that are the
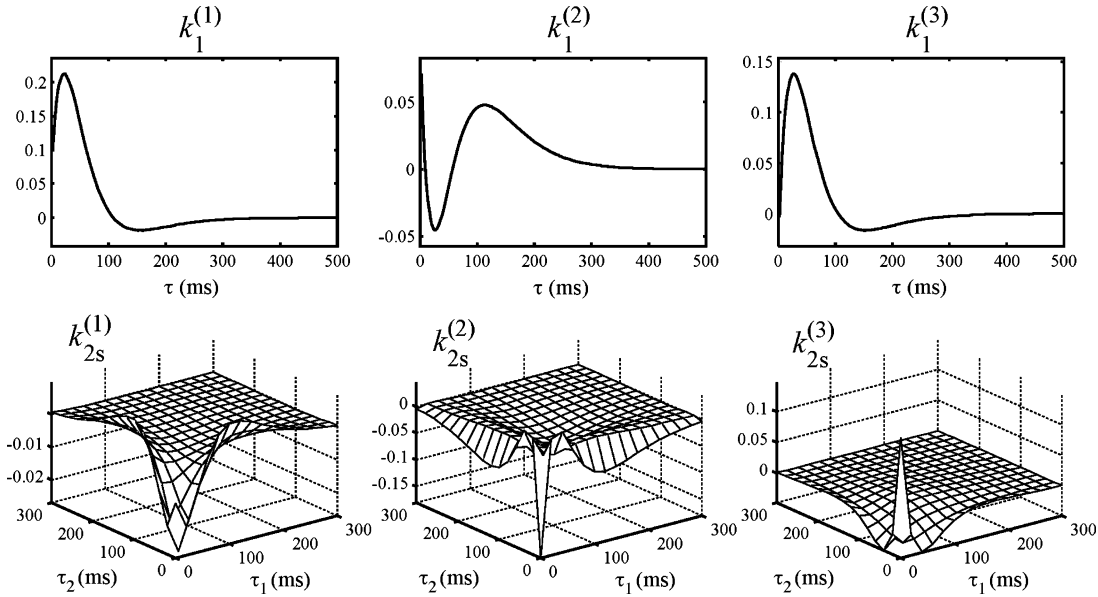
Fig. 5. Feedforward kernels of the second-order self-kernel model. First row: first-order kernels (k_1); second row: second-order self-kernels (k_{2s}). These kernels describe the pair-wise nonlinear interactions between spikes of the same input as they affect the hidden variable u. They are functions of the time intervals between present time and the previous pairs of spikes of the same input (τ_1 and τ_2). Each column of kernels corresponds to one input.
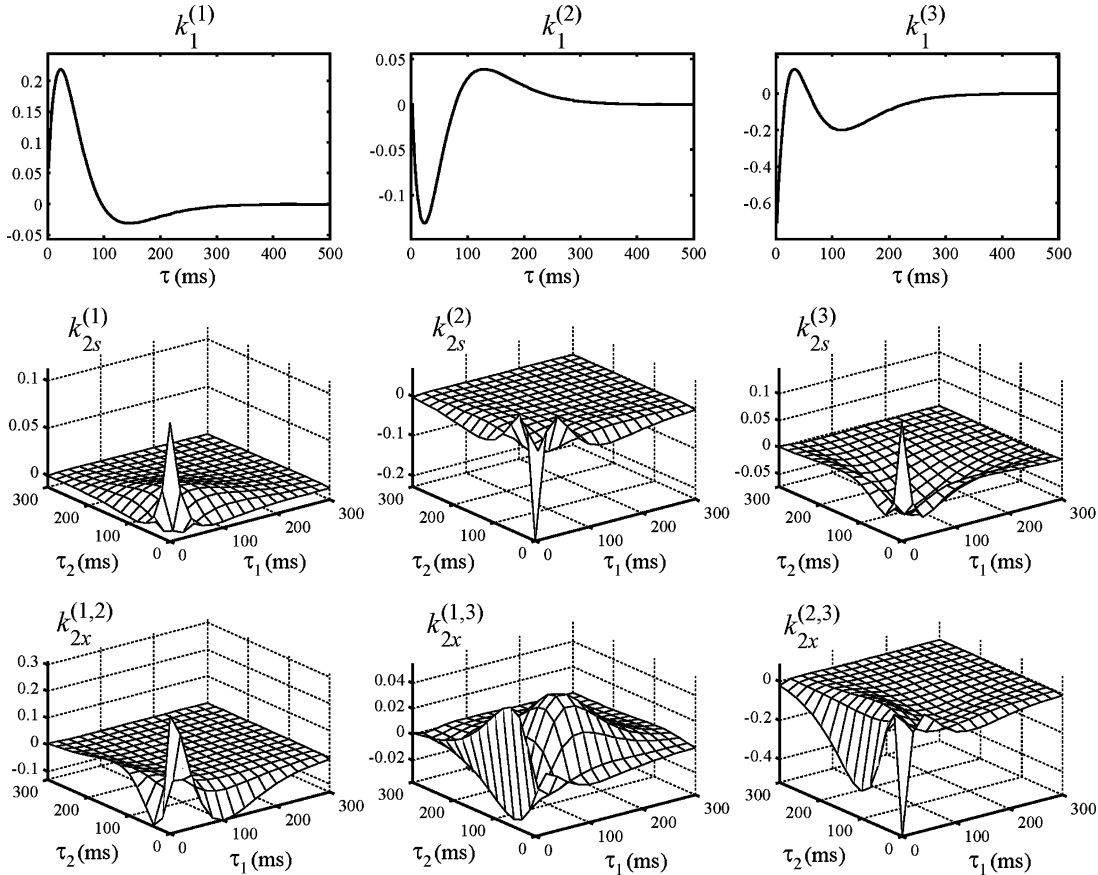

Fig. 6. Feedforward kernels of the second-order cross-kernel model. First row: first-order kernels (k_1); second row: second-order self-kernels (k_{2s}); third row: second-order cross-kernels (k_{2x}). These kernels describe the pair-wise nonlinear interactions between spikes of different inputs as they affect the hidden variable u. They are functions of the time intervals between present time and the previous pairs of spikes of different inputs (τ_1 and τ_2).

closest to the $45°$ line [Fig. 4(C)]. The maximum distance between model values and the $45°$ line is 0.056. All MISO datasets showed similar results (42 of 42).

Feedback kernels h of the four models are shown in Fig. 8. The h for all nonlinear models showed a similar shape, with a negative phase followed by a positive overshoot.
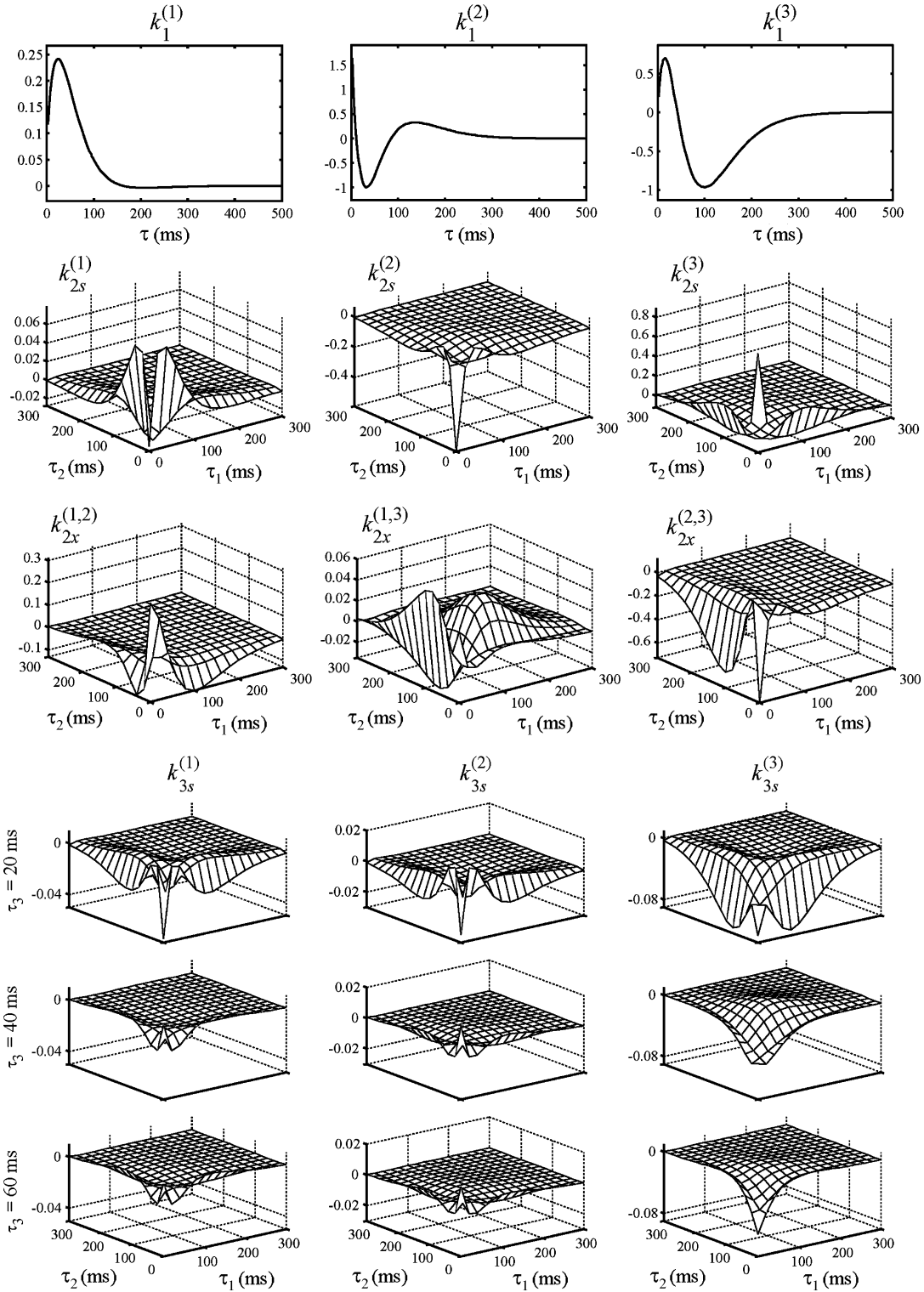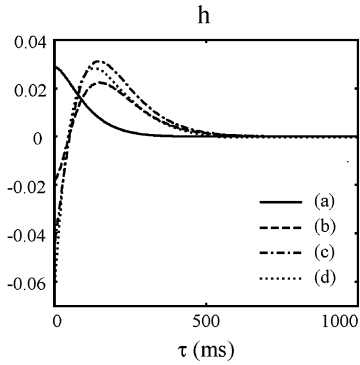
Fig. 7. Feedforward kernels of the third-order self-kernel model. First row: first-order kernels (k_1); second row: second-order self-kernels (k_{2s}); third row: second-order cross-kernels (k_{2x}); fourth to sixth rows: slices of third-order self-kernels (k_{3s}). These kernels describe the triplet-wise nonlinear interactions between spikes of the same input as they affect the hidden variable u. They are functions of three time intervals (τ_1, τ_2, and τ_3).

E. Model Prediction

All models described in this paper predict output (CA1) spike trains stochastically. Fig. 9 shows two trials of simulation with identical input spike trains x. The hidden variable u was deterministically predicted by the feedforward kernels given input x. Due to the randomly generated noise sequence, membrane potential w and consequently the predicted output spike train $\hat{y}$ show cross-trial variations (Fig. 9, trials A and B). The similarity between predicted output $\hat{y}$ and actual output y

Fig. 8. Feedback kernels (h) of (a) first-order kernel model, (b) second-order self-kernel model, (c) second-order cross-kernel model, and (d) third-order self-kernel model. h has a negative peak followed by a positive overshoot in all three nonlinear kernel models (b, c, and d). It describes the linear transformation of the output spike into the "after-potential" (a), as a function of the time interval between present time and previous output spikes (τ).
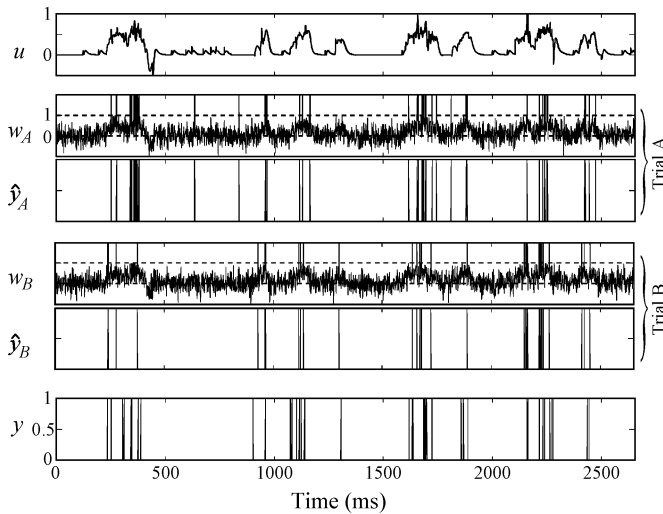

Fig. 9. Simulating output spike train with a MISO model. The hidden variable u was deterministically calculated from the input spike trains (x) and the feedforward kernels (K). Randomly generated white noise sequences were then added to u. Due to the stochastic nature of the model, different w and output spike trains ($\hat{y}_A$ and $\hat{y}_B$) were derived in trials of simulation (Trials A and B). y is the actual output spike train.

was quantified with a correlation measure involving a Gaussian kernel smoothing procedure. Correlation coefficients r were expressed as functions of the Gaussian smoothing kernel standard deviation σ_g (see Section II). Consistent with KS plot results, r results showed that the nonlinear kernel models were significantly more accurate than the linear kernel model in the whole range of σ_g [2–40 ms; Fig. 4(B)].

F. Predicting Spatio-Temporal Patterns With MIMO Models

Finally, MIMO kernel models were built by combining the individually identified MISO models. Each MISO model was validated and evaluated with a separate KS plot and correlation measure. Fig. 10 shows the second-order self-kernel MIMO model prediction for a 16-input, 7-output dataset. Results showed that the MIMO model successfully predicted the CA1 spatio-temporal pattern based on CA3 inputs, i.e., the MIMO kernels sufficiently capture the spatio-temporal pattern transformation from CA3 to CA1. MIMO models were successfully estimated for all animals (6 of 6).

IV. DISCUSSION

In sensory and other higher cortical brain regions, information is coded in the population activity of neurons. Any one neuron responds primarily to one feature of a larger set of features; it is the larger set of features that more accurately defines the "function" or "representation" of the population. The response of a single neuron to a given feature takes the form of a time series of action potentials, or a temporal pattern. Thus, the representation of the population takes the form of a spatio-temporal pattern. Understanding how the brain processes information requires understanding how spatio-temporal patterns of activity are progressively altered as "ensemble representations" propagate through the major sensory and higher cognitive pathways of the brain. Because the mechanisms underlying synaptic transmission are inherently nonlinear, achieving this goal requires methods for mathematical modeling nonlinear transformations of multiple point processes. Ultimately, the nonlinear, multiple-input, multiple-output model introduced here represents a critical step in realizing neural prostheses to replace damaged subregions of the hippocampus or any other central brain region. Prostheses for central brain regions many synapses removed from sensory transducers and motor effectors must include the very class of model introduced here, namely, one that replaces the transformation of multiple inputs into multiple outputs, where the inputs constitute the activity of afferents prior to the region of damage, and the outputs constitute the activity of neurons efferent to the region of damage.

Achieving a clinically viable prosthetic system that can replace the computational function of a region of hippocampus (or neocortex) requires more than the multiple-input, multiple-output model shown here. First, the model presented in the present paper is meant primarily to demonstrate the methodology and the feasibility for capturing up to third-order nonlinear dynamics for point-process input-output data. The present model could not be used in the context of a neural prosthesis until its generality has been tested fully, its sensitivity to context has been added, and modifiability of the model parameters has been included to account for learning [58]–[60]. In addition, fundamental issues related to hardware implementation and sensing/stimulating capability and biocompatibility will have to be resolved [12]. We view the present methodology as a significant step in the development of a prosthesis capable of replacing higher-thought processes such as memory, language, and planning/execution functions.

Here we introduced a physiologically plausible nonlinear dynamic kernel model for predicting an output spatio-temporal pattern of action potential events as a function of an input spatio-temporal pattern of action potential events for a synaptically connected population of neurons. We further demonstrated that this approach could be successfully applied to multi-site spike train data recorded from the hippocampus of behaving animals, specifically, CA3 spike train to CA1 spike train transformations during a memory task (DNMS) for the rat. Our results show that these transformations have significant nonlinearities that require at least second-order feedforward kernels. Models with more nonlinear terms, e.g., second-order cross-kernels and third-order self-kernels, resulted in a better fit to the output spike trains. Our results also show the existence of significant feedback, output spike-triggered dynamics of CA1 neurons.
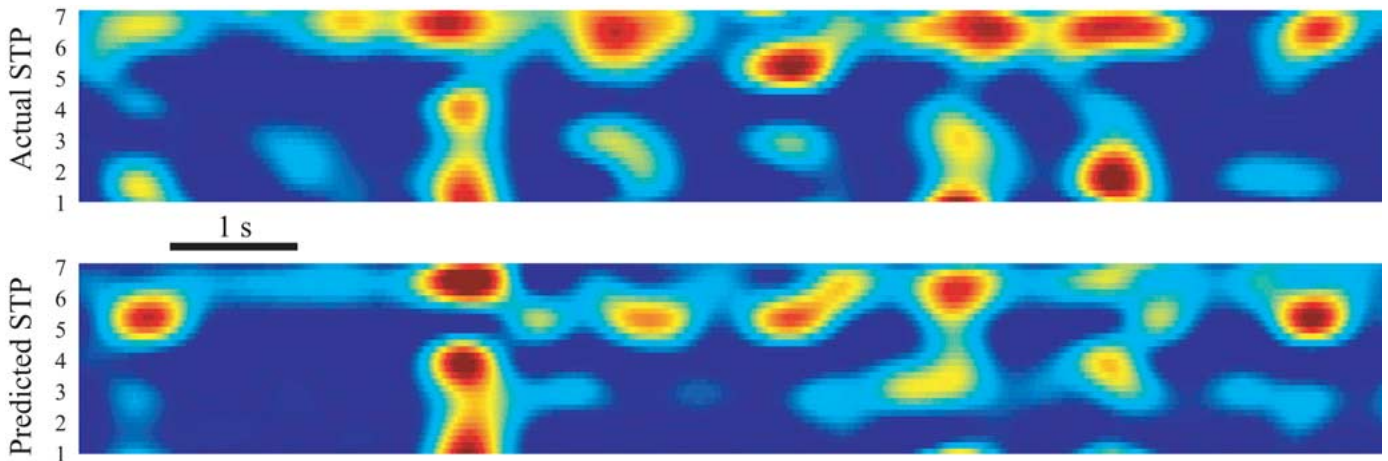
Fig. 10. Predicting output CA1 spatio-temporal pattern with a MIMO model. Spike trains were spatially and temporally interpolated for better visualization.

In the current model, intrinsic neuronal noise and the contribution of unobserved inputs were modeled as Gaussian white noise. Adding such a noise term to the model has important consequences. First, model predictions become stochastic. When the model is stochastic, directly matching the actual output to the predicted output is not a valid evaluation of the accuracy, or goodness-of-fit, of the model. Instead, it is more appropriate to evaluate such a model with respect to the statistical properties of its output, e.g., using a conditional firing intensity function. In general, comparisons between the precise timings of the actual output and predicted output are meaningful only when the system has a low noise level, i.e., small intrinsic neuronal noise *and* recording of the majority of inputs and, thus, can be adequately described by a deterministic model. These conditions are not met in our modeled system, especially given that only a small subset of system inputs, i.e., afferent CA3 spike trains, can be recorded for a given population of CA1 neurons. A second consequence of the noise term is that a maximum-likelihood function can be formulated to estimate model parameters. It is important to emphasize that, although after Laguerre expansion, hidden variables u and a are linearly related to the convolutions (and the products of those convolutions in the nonlinear models) of the inputs with Laguerre basis functions (v), and the noise is modeled as Gaussian, the maximum-likelihood estimation of the expansion coefficients (c) *cannot* be reduced to least-squares linear regression. The reason is that the system output consists of all-or-none spikes generated by thresholding the continuous hidden variable. The likelihood of observing actual output involves the error function, i.e., the integral of the Gaussian function, rather than the Gaussian function itself (see Section II-D). If the hidden variable w could be obtained experimentally, e.g., from intracellular recordings of CA1 neurons, c then could be more easily estimated using a linear regression technique.

The assumption of whiteness of the noise process in the model could be inaccurate under some circumstances, e.g., when the input spike trains are weakly correlated with the output spike train and the unobserved inputs have strong autocorrelations. We plan on considering the use of noise kernel(s) to model the correlated noise in future work. In the current model configuration scheme, the MIMO system was modeled as a series of MISO systems. This strategy works well but could be modified to be more efficient for a larger number of correlated outputs, e.g., using a canonical correlation analytical approach to reduce the dimensionality of both the input and the output simultaneously.

Interestingly, our results clearly revealed that different CA3-CA1 neuronal connections can exhibit markedly different forms of nonlinear dynamics, as represented by the very different first- and second-order kernel shapes. All of the neurons included in the present study were presumed hippocampal pyramidal neurons and interneurons, based on their firing rates and the location of recorded neurons relative to the physiologically identified pyramidal cell layer. This finding indicates a significant functional heterogeneity among hippocampal neurons and their synaptic circuitry, and demands further, systematic exploration of the anatomical, physiological, and other mechanisms underlying these differences to gain more insights into the re-encoding function of the hippocampus.

REFERENCES

[1] M. S. Humayun, E. de Juan, J. D. Weiland, G. Dagnelie, S. Katona, R. Greenberg, and S. Suzuki, "Pattern electrical stimulation of the human retina," *Visionn Res.*, vol. 39, pp. 2569–2576, 1999.

[2] G. E. Loeb, "Cochlear prosthetics," *Annu. Rev. Neurosci.*, vol. 13, pp. 357–371, 1990.

[3] G. E. Loeb, R. A. Peck, W. H. Moore, and K. Hood, "BIONTM system for distributed neural prosthetic interfaces," *Med. Eng. Phys.*, vol. 23, pp. 9–18, 2001.

[4] K. H. Mauritz and H. P. Peckham, "Restoration of grasping functions in quadriplegic patients by Functional Electrical Stimulation (FES)," *Int. J. Rehabil. Res.*, vol. 10, no. 4, Suppl. 5, pp. 57–61, 1987.

[5] J. P. Donoghue, "Connecting cortex to machines: Recent advances in brain interfaces," *Nature Neurosci.*, vol. 5, pp. 1085–1088, 2002.

[6] L. R. Hochberg, M. D. Serruya, G. M. Friehs, J. A. Mukand, M. Saleh, A. H. Caplan, A. Branner, D. Chen, R. D. Penn, and J. P. Donoghue, "Neuronal ensemble control of prosthetic devices by a human with tetraplegia," *Nature*, vol. 442, pp. 164–171, 2006.

[7] M. A. L. Nicolelis, "Brain-machine interfaces to restore motor function and probe neural circuits," *Nature Rev. Neurosci.*, vol. 4, pp. 417–422, 2003.

[8] K. V. Shenoy, D. Meeker, S. Y. Cao, S. A. Kureshi, B. Pesaran, C. A. Buneo, A. R. Batista, P. P. Mitra, J. W. Burdick, and R. A. Andersen, "Neural prosthetic control signals from plan activity," *Neuroreport*, vol. 14, pp. 591–596, 2003.

[9] D. M. Taylor, S. I. H. Tillery, and A. B. Schwartz, " Information conveyed through brain-control: cursor versus robot," *IEEE Trans. Neural Syst. Rehabil. Eng.*, vol. 11, no. 2, pp. 195–199, Jun. 2003.

[10] J. R. Wolpaw and D. J. McFarland, "Control of a two-dimensional movement signal by a noninvasive brain-computer interface in humans," in *Proc. Nat. Acad. Sci. USA*, 2004, vol. 101, pp. 17849–17854.

[11] T. W. Berger, A. Ahuja, S. H. Courellis, S. A. Deadwyler, G. Erinjip-purath, G. A. Gerhardt, G. Gholmieh, J. J. Granacki, R. Hampson, M. C. Hsaio, J. Lacoss, V. Z. Marmarelis, P. Nasiatka, V. Srinivasan, D. Song, A. R. Tanguay, and J. Wills, "Restoring lost cognitive function," *IEEE Eng. Med. Biol. Mag.*, vol. 24, no. 5, pp. 30–44, Sep.-Oct. 2005.

[12] T. W. Berger, M. Baudry, R. D. Brinton, J. S. Liaw, V. Z. Marmarelis, A. Y. Park, B. J. Sheu, and A. R. Tanguay, "Brain-implantable biomimetic electronics as the next era in neural prosthetics," *Proc. IEEE*, vol. 89, no. 7, pp. 993–1012, Jul. 2001.

[13] T. W. Berger, "Long-term potentiation of hippocampal synaptic transmission affects rate of behavioral learning," *Science*, vol. 224, pp. 627–630, 1984.

[14] T. W. Berger, B. Alger, and R. F. Thompson, "Neuronal substrate of classical-conditioning in hippocampus," *Science*, vol. 192, pp. 483–485, 1976.

[15] H. Eichenbaum, P. Dudchenko, E. Wood, M. Shapiro, and H. Tanila, "The hippocampus, memory, and place cells: Is it spatial memory or a memory space?," *Neuron*, vol. 23, pp. 209–226, 1999.

[16] M. L. Smith and B. Milner, "The role of the right hippocampus in the recall of spatial location," *Neuropsychologia*, vol. 19, p. 781, 1981, &.

[17] L. R. Squire, "Memory and the hippocampus - a synthesis from findings with rats, monkeys, and humans," *Psychological Rev.*, vol. 99, pp. 195–231, 1992.

[18] O. Bendel, T. Bueters, M. von Euler, S. O. Ogren, J. Sandin, and G. von Euler, "Reappearance of hippocampal CA1 neurons after ischemia is associated with recovery of learning and memory," *J. Cereb. Blood Flow Metab.*, vol. 25, pp. 1586–1595, 2005.

[19] S. Love, "Apoptosis and brain ischaemia," *Prog. Neuro-Psychopharmacol. Biol. Psych.*, vol. 27, pp. 267–282, 2003.

[20] A. L. Mccall, M. Moholtsiebert, A. Vanbueren, N. J. Cherry, N. Lessov, N. Tiffany, M. Thompson, H. Downes, and W. R. Woodward, "Progressive hippocampal loss of immunoreactive Glut3, the neuron-specific glucose-transporter, after global forebrain sschemia in the rat," *Brain Res.*, vol. 670, pp. 29–38, 1995.

[21] K. J. Sass, C. P. Buchanan, S. Kraemer, M. Westerveld, J. H. Kim, and D. D. Spencer, "Verbal memory impairment resulting from hippocampal neuron loss among epileptic patients with structural lesions," *Neurology*, vol. 45, pp. 2154–2158, 1995.

[22] D. H. Lowenstein, M. J. Thomas, D. H. Smith, and T. K. Mcintosh, "Selective vulnerability of dentate hilar neurons following traumatic brain injury—A potential mechanistic link between head trauma and disorders of the hippocampus," *J. Neurosci.*, vol. 12, pp. 4846–4853, 1992.

[23] G. Simic, I. Kostovic, B. Winblad, and N. Bogdanovic, "Volume and number of neurons of the human hippocampal formation in normal aging and Alzheimer's disease," *J. Comp. Neurol.*, vol. 379, pp. 482–494, 1997.

[24] T. Gomez-Isla, J. L. Price, D. W. McKeel, J. C. Morris, J. H. Growdon, and B. T. Hyman, "Profound loss of layer II entorhinal cortex neurons occurs in very mild Alzheimer's disease," *J. Neurosci.*, vol. 16, pp. 4491–4500, 1996.

[25] S. J. Teipel, J. C. Pruessner, F. Faltraco, C. Born, M. Rocha-Unold, A. Evans, H. J. Moller, and H. Hampel, "Comprehensive dissection of the medial temporal lobe in AD: Measurement of hippocampus, amygdala, entorhinal, perirhinal and parahippocampal cortices using MRI," *J. Neurol.*, vol. 253, pp. 794–800, 2006.

[26] A. Pouget, P. Dayan, and R. S. Zemel, "Inference and computation with population codes," *Annu. Rev. Neurosci.*, vol. 26, pp. 381–410, 2003.

[27] J. L. Puchalla, E. Schneidman, R. A. Harris, and M. J. Berry, "Redundancy in the population code of the retina," *Neuron*, vol. 46, pp. 493–504, 2005.

[28] A. P. Georgopoulos, A. B. Schwartz, and R. E. Kettner, "Neuronal population coding of movement direction," *Science*, vol. 233, pp. 1416–1419, 1986.

[29] A. B. Schwartz, R. E. Kettner, and A. P. Georgopoulos, "Primate motor cortex and free arm movements to visual targets in 3-dimensional space .1. Relations between single cell discharge and direction of movement," *J. Neurosci.*, vol. 8, pp. 2913–2927, 1988.

[30] F. P. Battaglia, G. R. Sutherland, and B. L. McNaughton, "Local sensory cues and place cell directionality: Additional evidence of prospective coding in the hippocampus," *J. Neurosci.*, vol. 24, pp. 4541–4550, 2004.

[31] H. Eichenbaum, M. Kuperstein, A. Fagan, and J. Nagode, "Cue-sampling and goal-approach correlates of hippocampal unit-activity in rats performing an odor-discrimination task," *J. Neurosci.*, vol. 7, pp. 716–732, 1987.

[32] J. R. Moyer, L. T. Thompson, and J. F. Disterhoft, "Trace eyeblink conditioning increases CA1 excitability in a transient and learning-specific manner," *J. Neurosci.*, vol. 16, pp. 5536–5546, 1996.

[33] D. L. Alkon, D. G. Amaral, M. F. Bear, J. Black, T. J. Carew, N. J. Cohen, J. F. Disterhoft, H. Eichenbaum, S. Golski, L. K. Gorman, G. Lynch, B. L. Mcnaughton, M. Mishkin, J. R. Moyer, J. L. Olds, D. S. Olton, T. Otto, L. R. Squire, U. Staubli, L. T. Thompson, and C. Wible, "Learning and memory," *Brain Research Reviews*, vol. 16, pp. 193–220, 1991.

[34] K. Nakazawa, M. C. Quirk, R. A. Chitwood, M. Watanabe, M. F. Yeckel, L. D. Sun, A. Kato, C. A. Carr, D. Johnston, M. A. Wilson, and S. Tonegawa, "Requirement for hippocampal CA3 NMDA receptors in associative memory recall," *Science*, vol. 297, pp. 211–218, 2002.

[35] S. A. Deadwyler and R. E. Hampson, "Ensemble activity and behavior—Whats the code?," *Science*, vol. 270, pp. 1316–1318, 1995.

[36] N. Burgess, E. A. Maguire, and J. O'Keefe, "The human hippocampus and spatial and episodic memory," *Neuron*, vol. 35, pp. 625–641, 2002.

[37] S. A. Deadwyler, T. Bunn, and R. E. Hampson, "Hippocampal ensemble activity during spatial delayed-nonmatch-to-sample performance in rats," *J. Neurosci.*, vol. 16, pp. 354–372, 1996.

[38] D. Song, V. Z. Marmarelis, and T. W. Berger, "Parametric and nonparametric models of short-term plasticity," in *Proc. 2nd Joint EMBS/BMES Conf.*, 2002, vol. 3, pp. 1964–1965.

[39] R. S. Zucker and W. G. Regehr, "Short-term synaptic plasticity," *Annu. Rev. Physiol.*, vol. 64, pp. 355–405, 2002.

[40] P. Poirazi, T. Brannon, and B. W. Mel, "Arithmetic of subthreshold synaptic summation in a model CA1 pyramidal cell," *Neuron*, vol. 37, pp. 977–987, 2003.

[41] B. E. Alger and R. A. Nicoll, "Pharmacological evidence for two kinds of GABA receptor on rat hippocampal pyramidal cells studied *in vitro*," *J. Physiol.*, vol. 328, pp. 125–141, 1982.

[42] T. W. Berger, G. Chauvet, and R. J. Sclabassi, "A biological based model of functional properties of the hippocampus," *Neural Netw.*, vol. 7, pp. 1031–1064, 1994.

[43] J. Keat, P. Reinagel, R. C. Reid, and M. Meister, "Predicting every spike: A model for the responses of visual neurons," *Neuron*, vol. 30, pp. 803–817, 2001.

[44] L. Paninski, J. W. Pillow, and E. P. Simoncelli, "Maximum likelihood estimation of a stochastic integrate-and-fire neural encoding model," *Neural Computation*, vol. 16, pp. 2533–2561, 2004.

[45] D. Song, Z. Wang, and T. W. Berger, "Contribution of T-type VDCC to TEA-induced long-term synaptic modification in hippocampal CA1 and dentate gyrus," *Hippocampus*, vol. 12, pp. 689–697, 2002.

[46] J. F. Storm, "Action potential repolarization and a fast after-hyperpolarization in rat hippocampal pyramidal cells," *J. Physiol.*, vol. 385, pp. 733–759, 1987.

[47] R. E. Hampson, J. D. Simeral, and S. A. Deadwyler, "Distribution of spatial and nonspatial information in dorsal hippocampus.," *Nature*, vol. 402, pp. 610–614, 1999.

[48] V. Volterra, *Theory of functionals and of integral and integro-differential equations*. New York: Dover, 1959.

[49] V. Z. Marmarelis and P. Z. Marmarelis, *Analysis of Physiological Systems: The White-Noise Approach*. New York: Plenum, 1978.

[50] V. Z. Marmarelis, *Nonlinear Dynamic Modeling of Physiological Systems*. Hoboken, NJ: Wiley-IEEE Press, 2004.

[51] V. Z. Marmarelis, "Signal transformation and coding in neural systems," *IEEE Trans. Biomed. Eng.*, vol. 36, no. 1, pp. 15–24, Jan. 1989.

[52] V. Z. Marmarelis and M. E. Orme, "Modeling of neural systems by use of neuronal modes," *IEEE Trans. Biomed. Eng.*, vol. 40, no. 11, pp. 1149–1158, Nov. 1993.

[53] C. M. Bishop, *Neural Networks for Pattern Recognition*. Oxford, U.K.: Oxford Univ. Press, 1995.

[54] W. Truccolo, U. T. Eden, M. R. Fellows, J. P. Donoghue, and E. N. Brown, "A point process framework for relating neural spiking activity to spiking history, neural ensemble, and extrinsic covariate effects," *J. Neurophysiol.*, vol. 93, pp. 1074–1089, 2005.

[55] M. H. Kutner, C. J. Nachtsheim, J. Neter, and W. Li, *Applied Linear Statistical Models*, 5th ed. Boston, MA: McGraw-Hill/Irwin, 2004.

[56] E. N. Brown, R. Barbieri, V. Ventura, R. E. Kass, and L. M. Frank, "The time-rescaling theorem and its application to neural spike train data analysis," *Neural Computation*, vol. 14, pp. 325–346, 2002.

[57] L. W. Swanson, J. M. Wyss, and W. M. Cowan, "An autoradiographic study of the organization of intrahippocampal association pathways in the rat," *J. Comp. Neurol.*, vol. 181, pp. 681–715, 1978.

[58] M. Iatrou, T. Berger, and V. Z. Marmarelis, "Modeling of nonlinear nonstationary dynamic systems with a novel class of artificial neural networks," *IEEE Trans. Neural Netw.*, vol. 10, no. 2, pp. 327–339, Mar. 1999.

[59] M. Iatrou, T. W. Berger, and V. Z. Marmarelis, "Application of a novel modeling method to the nonstationary properties of potentiation in the rabbit hippocampus," *Ann. Biomed. Eng.*, vol. 27, pp. 581–591, 1999.

[60] D. Krieger, T. W. Berger, and R. J. Sclabassi, "Instantaneous characterization of time-varying nonlinear systems," *IEEE Trans. Biomed. Eng.*, vol. 39, no. 4, pp. 420–424, Apr. 1992.

Vasilis Z. Marmarelis (M'79–SM'94–F'97) was born in Mytiline, Greece, on November 16, 1949. He received the Diploma degree in electrical engineering and mechanical engineering from the National Technical University of Athens, Athens, Greece, in 1972 and the M.S. and Ph.D. degrees in engineering science (information science and bioinformation systems) from the California Institute of Technology, Pasadena, in 1973 and 1976, respectively.

After two years of postdoctoral work at the California Institute of Technology, he joined the faculty of Biomedical and Electrical Engineering at the University of Southern California, Los Angeles, where he is currently Professor and Director of the Biomedical Simulations Resource, a research center funded by the National Institutes of Health since 1985 and dedicated to modeling/simulation studies of biomedical systems. He served as Chairman of the Biomedical Engineering Department from 1990 to 1996. His main research interests are in the areas of nonlinear and nonstationary system identification and modeling, with applications to biology and medicine. His other interests include spatio-temporal and multi-input/multi-output modeling of nonlinear systems, with applications to neural information processing, closed-loop system modeling and high-resolution 3D ultrasonic imaging and tissue classification. He is co-author of *Analysis of Physiological System: The White Noise Approach* (Plenum, 1978; Russian translation: Moscow, Mir Press, 1981; Chinese translation: Academy of Sciences Press, Beijing, 1990), editor of three research volumes on *Advanced Methods of Physiological System Modeling* (Plenum, 1987, 1989, 1994) and author of a monograph on *Nonlinear Dynamic Modeling of Physiological Systems* (IEEE Press & Wiley Interscience, 2004). He has published more than 100 papers and book chapters in the areas of system modeling and signal analysis.

Dr. Marmarelis is a Fellow of the American Institute for Medical and Biological Engineering.

Dong Song (S'02–M'04) received the B.S. degree in biophysics from the University of Science and Technology of China, Hefei, China, in 1994 and the Ph.D. degree in biomedical engineering from the University of Southern California (USC), Los Angeles, in 2003.

From 2004–2006, he worked as a Postdoctoral Research Associate at the Center for Neural Engineering at USC. He is currently a Research Assistant Professor at the Department of Biomedical Engineering at USC. His main research interests include nonlinear systems analysis of nervous system, cortical neural prosthesis, electrophysiology of hippocampus, long-term and short-term synaptic plasticity, and the development of modeling methods incorporating both parametric and nonparametric modeling techniques.

Dr. Song is a member of Biomedical Engineering Society and Society for Neuroscience.

Robert E. Hampson received his Ph.D. degree from Wake Forest University in 1988 in physiology.

He was a postdoctoral fellow and assistant professor at that institution from 1989–1998 when he was promoted to the rank of associate professor. He is an Associate Professor in the Department of Physiology and Pharmacology, Wake Forest University School of Medicine Winston-Salem, NC. He is a past member of the IFCN-7 National Institutes of Health (NIH) review panel and has served as an ad hoc member of other review panels for NIH. His main interests are in learning and memory: in particular deciphering the neural code utilized by the hippocampus and other related structures to encode behavioral events and cognitive decisions. His other interests are in linear and nonlinear modeling of neural encoding of cognitive processes as well as alterations of that encoding by drugs of abuse. He has published extensively in the areas of cannabinoid effects on behavior and electrophysiology, and the correlation of behavior with multineuron activity patterns, particularly applying linear discriminant analysis to neural data to decipher population encoding and representation.

Rosa H. M. Chan received the B.Eng. degree in automation and computer-aided engineering from the Chinese University of Hong Kong (CUHK), Hong Kong, in 2003. Awarded by both Croucher Scholarship and Sir Edward Youde Memorial Fellowship for overseas study, she is currently working towards the Ph.D. degree in the Department of Biomedical Engineering of University of Southern California.

In 2001, she studied in the New York University for computer animation and visual effects supported by Hong Kong Productivity Council and Film Development Fund. Funded by the scholarship from the Association of International Exchange, Japan, she joined the University Mobility in Asia and the Pacific (UMAP) Leaders Program and worked in the Aerospace Applied Physics Laboratory of the Department of Aeronautics and Astronautics at Kyushu University in 2002. Her research interest is in the development of cortical neural prosthesis.

Ms. Chan is a student member of Hong Kong Institution of Engineers (HKIE). She also received the undergraduate scholarship from the HKIE Manufacturing and Industrial Engineering Division in 2003.

Samuel A. Deadwyler received his Ph.D. from the State University of New York, Stony Brook and conducted postdoctoral research at the University of California, Irvine.

He is a Professor with the Department of Physiology and Pharmacology, Wake Forest University School of Medicine (WFUSM), Winston-Salem, NC, where he has been since 1978. He has been funded by the National Institutes of Health (NIH) continuously since 1974. He is on the editorial board of the journal *Hippocampus* and has been an invited Grass Foundation lecturer on several different occasions. He is past president of the International Cannabinoid Research Society and was elected to the Board of Directors of the College on Problems of Drug Dependence for a 4 year term. He has published extensively in journal articles, chapters, and books on his research into neural mechanisms of learning and memory as well as cellular neurophysiological investigation of drug actions. His research interests include mechanisms of information encoding in neuronal populations,

relationship between neuronal codes and behavioral performance, mechanisms of enhancement of short-term memory in relation to neural codes generated in the hippocampus and frontal cortex.

Dr. Deadwyler is the recipient of a NIH Senior Research Scientist award from 1987–2008 and also a MERIT award from 1990–2000. He served on the editorial board for the *Journal of Neuroscience* from 1996–2005 during which time he was also a reviewing editor.

Theodore W. Berger (M'03–SM'04) received his Ph.D. from Harvard University in 1976; his thesis work received the James McKeen Cattell Award from the New York Academy of Sciences.

He is the David Packard Professor of Engineering, Professor of Biomedical Engineering and Neuroscience, and Director of the Center for Neural Engineering at the University of Southern California. He conducted postdoctoral research at the University of California, Irvine from 1977–1978, and was an Alfred P. Sloan Foundation Fellow at the Salk Institute from 1978–1979. He joined the Departments of Neuroscience and Psychiatry at the University of Pittsburgh, Pittsburgh, PA, in 1979, being promoted through to Full Professor in 1987. Since 1992, he has been Professor of Biomedical Engineering and Neurobiology at the University of Southern California (USC), and was appointed the David Packard Chair of Engineering in 2003. He has published over 170 journal articles and book chapters, and is the co-editor of *Toward Replacement Parts for the Brain: Implantable Biomimetic Electronics as Neural Prostheses* (MIT Press, 2005. His research interests are in the development of biologically realistic, experimentally-based, mathematical models of higher brain (hippocampus) function, application of biologically realistic neural network models to real-world signal processing problems, VLSI-based implementations of biologically realistic models of higher brain function, neuron-silicon interfaces for bi-directional communication between brain and VLSI systems, and next-generation brain-implantable, biomimetic signal processing devices for neural prosthetic replacement and/or enhancement of brain function.

Dr. Berger received a McKnight Foundation Scholar Award, twice received an NIMH Research Scientist Development Award, and was elected a Fellow of the American Association for the Advancement of Science. While at USC, he has received an NIMH Senior Scientist Award, was given the Lockheed Senior Research Award in 1997, was elected a Fellow of the American Institute for Medical and Biological Engineering in 1998, received a Person of the Year "Impact Award" by the AARP in 2004 for his work on neural prostheses, was a National Academy of Sciences International Scientist Lecturer in 2003, and an IEEE Distinguished Lecturer in 2004–2005. He was elected a Senior Member of the IEEE in 2005, received a "Great Minds, Great Ideas" award from the EE Times in the same year, and in 2006 was awarded USC's Associates Award for Creativity in Research and Scholarship. He became Director of the Center for Neural Engineering in 1997, an organization which helps to unite USC faculty with cross-disciplinary interests in neuroscience, engineering, and medicine.